J. Phys. Chem. A **2003,** *107,* 4147−4150

^{57}Fe Mössbauer Quadrupole Splittings and Isomer Shifts in Spin-Crossover Complexes: A Density Functional Theory Investigation

Yong Zhang and Eric Oldfield*

Departments of Chemistry and Biophysics, University of Illinois at Urbana-Champaign,
600 South Mathews Avenue, Urbana, Illinois 61801

Received: February 18, 2003; In Final Form: March 24, 2003

We report the results of density functional theory (DFT) calculations of the ^{57}Fe Mössbauer quadrupole splittings ΔE_Q and isomer shifts δ_{Fe} of both the high-spin (HS) and low-spin (LS) states of two typical spin crossover complexes: the six-coordinate species *cis*-bis(thiocyanato)bis(1,10-phenanthroline)iron(II), (Fe(phen)$_2$(NCS)$_2$; $S = 2$ or 0) and the five-coordinate system, [*N*,*N*′-ethylenebis(salicylideniminato)]nitrosyl iron(II), (Fe(salen)(NO); $S = 3/2$ or 1/2). There is excellent agreement between the experimental data and the theoretical calculations. The wave functions derived are used to clarify some aspects of the differences between the HS and LS electronic states of these materials, and they put on a firm theoretical foundation the use of Mössbauer spectroscopy to investigate spin-crossover complexes.

Introduction

One of the most appealing aspects of molecular materials science is to utilize and/or design specific types of molecules or molecular assemblies for information processing and storage. To fulfill such a task, molecules need to exhibit bistability, for example by existing in distinct electronic states as a function of an external perturbation. Due to bistability between high-spin (HS) and low-spin (LS) states, spin-crossover complexes are of considerable interest since bistability can be readily manipulated by means of temperature, pressure or illumination,[1] and spin-crossover complexes have attracted much interest since their discovery in the 1930s.[2−7] The recent synthesis of room-temperature spin-crossover complexes[8,9] has greatly stimulated both fundamental studies and potential applications. However, when compared with the large amount of experimental work in this area, theoretical studies have been scarce[10−14] and have mainly focused on thermal parameters, such as equilibrium geometries, energies, and normal modes of vibration. There are, however, a number of ^{57}Fe Mössbauer spectroscopic results on these systems which might also be amenable to theoretical analysis since molecular orbital calculations have recently been successfully employed in the investigation of the Mössbauer spectra of other complex species, such as iron porphyrins and related compounds.[15−19] Here, we therefore report the first applications of density functional theory (DFT) methods to predict two spectroscopic observables in the HS and LS states of two archetypal spin-crossover complexes: *cis*-bis(thiocyanato)bis(1,10-phenanthroline)iron(II) (Fe(phen)$_2$(NCS)$_2$) and [*N*,*N*′-ethylene bis(salicylideniminato)]nitrosyl iron (II) (Fe(salen)(NO)), as shown in Figure 1. The X-ray structures of both species have previously been obtained at both high and low temperatures as have their ^{57}Fe Mössbauer spectra,[20−23] and the spectroscopic observables cover a wide range: from 0.34 to 2.67 mm s^{-1} for ΔE_Q and from 0.28 to 0.98 mm s^{-1} for δ_{Fe}, providing a good test of the theoretical predictions, and hence of the computed wave functions.

Computational Aspects

The ^{57}Fe quadrupole splitting arises from the nonspherical nuclear charge distribution in the $I^* = 3/2$ excited state in the presence of an electric field gradient at the ^{57}Fe nucleus, while the isomer shift arises from differences in the electron density at the nucleus between the absorber (the molecule or system of interest) and a reference compound (usually α-Fe at 300 K). The former effect is related to the components of the electric field gradient tensor at the nucleus as follows:[24]

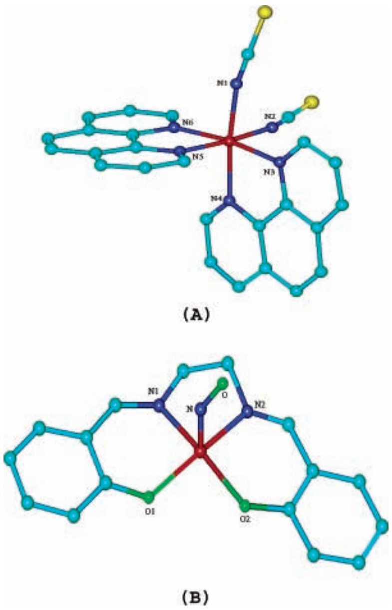

Figure 1. Molecular structures of (A) Fe(phen)$_2$(NCS)$_2$ and (B) Fe(salen)(NO) with hydrogen atoms eliminated for clarity. The color scheme is as follows: Fe, red; N, blue; C, cyan; O, green; S, yellow.

$$\Delta E_Q = \frac{1}{2} eQV_{zz}\left(1 + \frac{\eta^2}{3}\right)^{1/2} \tag{1}$$

where e is the electron charge, Q is the quadrupole moment of the $E^* = 14.4$ keV excited state, and the principal components of the EFG tensor are labeled according to the convention:

$$|V_{zz}| > |V_{yy}| > |V_{xx}| \tag{2}$$

10.1021/jp030222u CCC: \$25.00

with the asymmetry parameter being given by:

$$\eta = \frac{V_{xx} - V_{yy}}{V_{zz}}. \tag{3}$$

The isomer shift in ^{57}Fe Mössbauer spectroscopy is given by:[24]

$$\delta_{\mathrm{Fe}} = E_{\mathrm{A}} - E_{\mathrm{Fe}} = \frac{2\pi}{3} Ze^2(\langle R^2\rangle^* - \langle R^2\rangle)(|\psi(0)|_{\mathrm{A}}^2 - |\psi(0)|_{\mathrm{Fe}}{}^2) \tag{4}$$

where Z represents the atomic number of the nucleus of interest (iron) and R and R^* are average nuclear radii of the ground and excited states of ^{57}Fe. Since $|\psi(0)|_{\mathrm{Fe}}{}^2$ is a constant, the isomer shift (from Fe) can be written as

$$\delta_{\mathrm{Fe}} = \alpha[\rho(0) - c] \tag{5}$$

where α is the so-called calibration constant and $\rho(0)$ is the computed charge density at the iron nucleus. Both α and c can be obtained from the correlation between experimental δ_{Fe} values and the corresponding computed $\rho(0)$ data in a training set and are dependent on the quantum chemical method used and the choice of basis set.[19] Then, one can use eq 5 to predict δ_{Fe} for a new molecule from its computed $\rho(0)$, basically as described in detail elsewhere for a wide variety of heme and other model systems.[19]

To calculate ΔE_{Q}, we used the Gaussian 98 program[25] to evaluate the principal components of the electric field gradient tensor at the ^{57}Fe nucleus V_{ii} and then used eq 1 to deduce ΔE_{Q}, using the most precise recent determination[26] of $Q = 0.16$ (±5%) × 10^{-28}, a value previously found to permit excellent accord between theory and experiment in a broad range of systems.[16−18] We used the same computational approach as in our previous studies,[18−19,27] which enabled accurate predictions of Mössbauer quadrupole splittings and isomer shifts as well as NMR hyperfine shifts in iron complexes containing d^2 to d^8 iron and all spin states ($S = 0$, 1/2, 1, 3/2, 2, or 5/2): a Wachter's basis (62111111/3311111/3111)[28] for Fe, 6-311G* for all the other heavy atoms and 6-31G* for hydrogens. We investigated use of both the pure density functional BPW91 (Becke 88 exchange[29] and PW91[30] correlation functionals) as well as the hybrid functional B3LYP (Becke's three-parameter functional[31] with the LYP[32] correlation functional).

To calculate δ_{Fe} values, we read the wave functions from the Gaussian 98 calculations into the AIM 2000 program,[33] in order to evaluate the charge density at the iron nucleus, $\rho(0)$. Then, we evaluated the isomer shifts by using the two equations derived previously:[19]

$$\delta_{\mathrm{Fe}} = -0.471[\rho(0) - 11617.30](\mathrm{BPW91}) \tag{6}$$

$$\delta_{\mathrm{Fe}} = -0.404[\rho(0) - 11614.16](\mathrm{B3LYP}). \tag{7}$$

For Fe(phen)$_2$(NCS)$_2$, the X-ray structures[20] obtained at 293 K (high temperature (HT), HS) and 130 K (low temperature (LT), LS) were employed and the results compared with Mössbauer data[21] recorded at 293 and 77 K, respectively. For Fe(salen)(NO), single-crystal X-ray structures[22] determined at 296 K (HT, HS) and 98 K (LT, LS) were used and the results compared with Mössbauer data[23] recorded at 275 and 4.2 K, respectively. The NO structures exhibit crystallographic disorder with there being two NO positions in each spin state. All structures were considered in the property calculations and were weighted by their respective contributions. Both spin-crossover complexes have transition temperatures of ∼175 K.[20−23]

TABLE 1: Experimental and Computational Data for Fe(phen)$_2$(NCS)$_2$

method	structure:	RT[a]	LT[a]
	spin:	2	0
	Fe−N1 (Å)	2.057	1.958
	Fe−N2 (Å)	2.057	1.957
	Fe−N3 (Å)	2.198	2.013
	Fe−N4 (Å)	2.212	2.004
	Fe−N5 (Å)	2.212	2.005
	Fe−N6 (Å)	2.198	2.014
	N1−Fe−N2 (deg)	94.8	90.6
	N3−Fe−N4 (deg)	76.1	81.8
	N5−Fe−N6 (deg)	76.1	81.7
B3LYP	$\Delta E_{\mathrm{Q}}{}^{\mathrm{exp}}$ (mm s^{-1})[b]	(−)2.67	(+)0.34
	$\Delta E_{\mathrm{Q}}{}^{\mathrm{cal}}$ (mm s^{-1})[b]	−2.85	+0.32
	η^{cal} [b]	0.41	0.29
	$\delta_{\mathrm{Fe}}{}^{\mathrm{exp}}$ (mm s^{-1})[c]	0.98	0.37
	$\delta_{\mathrm{Fe}}{}^{\mathrm{cal}}$ (mm s^{-1})[c]	1.03	0.55
	$\rho(0)$ (au)	11611.62	11612.81
	$\rho_{\alpha\beta}{}^{\mathrm{Fe}}$ (e)[d]	3.80	0.00
BPW91	$\Delta E_{\mathrm{Q}}{}^{\mathrm{exp}}$ (mm s^{-1})[b]	(−)2.67	(+)0.34
	$\Delta E_{\mathrm{Q}}{}^{\mathrm{cal}}$ (mm s^{-1})[b]	−1.71	+0.53
	η^{cal} [b]	0.52	0.99
	$\delta_{\mathrm{Fe}}{}^{\mathrm{exp}}$ (mm s^{-1})[c]	0.98	0.37
	$\delta_{\mathrm{Fe}}{}^{\mathrm{cal}}$ (mm s^{-1})[c]	1.03	0.48
	$\rho(0)$ (au)	11615.12	11616.28
	$\rho_{\alpha\beta}{}^{\mathrm{Fe}}$ (e)[d]	3.74	0.00

[a] Crystal structures from ref 20. [b] The experimental quadrupole splittings $\Delta E_{\mathrm{Q}}{}^{\mathrm{exp}}$ are from ref 21 (unsigned), and their signs shown in parentheses are based on the calculated quadrupole splittings $\Delta E_{\mathrm{Q}}{}^{\mathrm{cal}}$. The calculated asymmetry parameter is labeled as η^{cal}. [c] $\delta_{\mathrm{Fe}}{}^{\mathrm{exp}}$ and $\delta_{\mathrm{Fe}}{}^{\mathrm{cal}}$ are the experimental (from ref 21) and calculated isomer shifts, respectively. [d] $\rho_{\alpha\beta}{}^{\mathrm{Fe}}$ is the Mulliken spin density of iron.

Spin-unrestricted methods were used for all property calculations. For Gaussian 98 calculations, Silicon Graphics (Mountain View, CA) O-300 and O-2000 computers were employed using typically eight (O-300) or 16 (O-2000) processors.

Results and Discussion

The experimental and computational results for ΔE_{Q} and δ_{Fe} for Fe(phen)$_2$(NCS)$_2$ are given in Table 1 and for Fe(salen)(NO), the experimental and computational results are presented in Table 2. Quite clearly, there is excellent accord between theory and experiment when using the hybrid exchange correlation functional (B3LYP) and the basis set scheme reported previously for metalloporphyrins.[18,19] For example, with Fe(phen)$_2$(NCS)$_2$, Table 1, the experimental (predicted) ΔE_{Q} values are (−)2.67 (−2.85) mm s^{-1} for the HS ($S = 2$) complex and (+)0.34 (+0.32) mm s^{-1} for the LS ($S = 0$) complex. The experimental results were not signed. However, there is excellent accord between computationally and experimentally determined signs in a wide range of other iron complexes, as described previously.[18,19] Likewise, the δ_{Fe} experimental (predicted) values are 0.98 (+1.03) mm s^{-1} for the HS ($S = 2$) complex and 0.37 (+0.55) mm s^{-1} for the LS ($S = 0$) complex. Overall, when considering both states of both types of spin crossover molecules, the average errors between theory and experiment are ∼0.095 mm s^{-1} for ΔE_{Q} and ∼0.11 mm s^{-1} for δ_{Fe} when using the B3LYP functional. The ΔE_{Q} error increases to ∼0.58 mm s^{-1} when using the BPW91 functional, and indeed, in previous work, we found a slight improvement in 23 ΔE_{Q} predictions when using this hybrid XC functional.[18] We have also found that the B3LYP functional in general provides the best correlations between theory and experiment for other properties as well,

TABLE 2: Experimental and Computational Data for Fe(NO)(salen)

method	structure:	LT1 (43 %)[a]	LT2 (57 %)[a]	RT1 (50 %)[a]	RT2 (50 %)[a]
	spin:	1/2	1/2	3/2	3/2
	Fe−N1 (Å)	1.978	1.978	2.084	2.084
	Fe−N2 (Å)	1.965	1.965	2.066	2.066
	Fe−O1 (Å)	1.928	1.928	1.923	1.923
	Fe−O2 (Å)	1.867	1.867	1.893	1.893
	Fe−N (Å)	1.792	1.810	1.782	1.782
	N−O (Å)	1.155	1.150	1.112	1.089
	Fe−N−O (deg)	133.9	122.6	144.1	149.9
B3LYP	ΔE_Q^{exp} (mm s^{-1})[b]	(+)1.950		(+)0.352	
	$^{av}\Delta E_Q^{cal}$ (mm s^{-1})[b]	+1.88		+0.46	
	ΔE_Q^{cal} (mm s^{-1})[b]	+1.74	+1.99	+0.40	+0.52
	η^{cal} [b]	0.90	0.87	0.48	0.54
	δ_{Fe}^{exp} (mm s^{-1})[c]	0.281		0.440	
	$^{av}\delta_{Fe}^{cal}$ (mm s^{-1})[c]	0.34		0.59	
	$\rho(0)$ (au)	11613.32	11613.33	11612.74	11612.66
	δ_{Fe}^{cal} (mm s^{-1})[c]	0.34	0.34	0.57	0.61
	$\rho_{\alpha\beta}^{Fe}$ (e)[d]	0.81	0.67	3.66	3.65
	$\rho_{\alpha\beta}^{NO}$ (e)[d]	0.19	0.33	−1.10	−1.08
BPW91	ΔE_Q^{exp} (mm s^{-1})[b]	(+)1.950		(+)0.352	
	$^{av}\Delta E_Q^{cal}$ (mm s^{-1})[b]	+1.67		+0.55	
	ΔE_Q^{cal} (mm s^{-1})[b]	+1.53	+1.77	+0.56	+0.54
	η^{cal} [b]	0.95	0.40	0.83	0.99
	δ_{Fe}^{exp} (mm s^{-1})[c]	0.281		0.440	
	$^{av}\delta_{Fe}^{cal}$ (mm s^{-1})[c]	0.37		0.66	
	$\rho(0)$ (au)	11616.50	11616.51	11615.94	11615.86
	δ_{Fe}^{cal} (mm s^{-1})[c]	0.38	0.37	0.64	0.68
	$\rho_{\alpha\beta}^{Fe}$ (e)[d]	1.12	1.19	3.13	3.13
	$\rho_{\alpha\beta}^{NO}$ (e)[d]	−0.19	−0.26	−0.76	−0.64

[a] Crystal structures from ref 22. The fractions of the disordered positions in RT and LT structures are shown in parentheses. [b] The experimental quadrupole splittings ΔE_Q^{exp} are from ref 23 (unsigned), and their signs shown in parentheses are based on the calculated quadrupole splittings ΔE_Q^{cal}. $^{av}\Delta E_Q^{cal}$ is the average computed quadrupole splitting weighted by the structural fraction. The calculated asymmetry parameter is labeled as η^{cal}. [c] δ_{Fe}^{exp} and δ_{Fe}^{cal} are the experimental (from ref 23) and calculated isomer shifts, respectively. $^{av}\delta_{Fe}^{cal}$ is the average computed isomers shift weighted by the structural fraction. [d] $\rho_{\alpha\beta}^{Fe}$ and $\rho_{\alpha\beta}^{NO}$ are the Mulliken spin densities of iron and the nitrosyl moiety.

such as NMR hyperfine shifts.[27] The δ_{Fe} error remains about the same, however, at ~0.12 mm s^{-1}.

Since the 130 K X-ray crystal structure for LS Fe(phen)$_2$(NCS)$_2$ contains a HS fraction of 17%,[20] we next estimated the isomer shift for a pure LS state (δ_{Fe}^{LS}) as follows:

$$x\delta_{Fe}^{HS} + (1 - x)\delta_{Fe}^{LS} = \delta_{Fe}^{130K} \tag{8}$$

where $x = 17\%$ is the HS impurity and δ_{Fe}^{HS} and δ_{Fe}^{130K} are the calculated isomer shifts for the experimental HS/293 K structure and LS/130 K structure respectively, as reported in Table 1. In this way, compared to the previously calculated δ_{Fe}^{130K} value of 0.55 (0.48) mm s^{-1} using B3LYP (BPW91), the predicted δ_{Fe}^{LS} becomes 0.45 (0.37) mm s^{-1} using B3LYP (BPW91), which is in much better agreement with the experimental 77 K Mössbauer measurement (0.37 mm s^{-1})[21] and reduces the prediction error by ~0.1 mm s^{-1}.

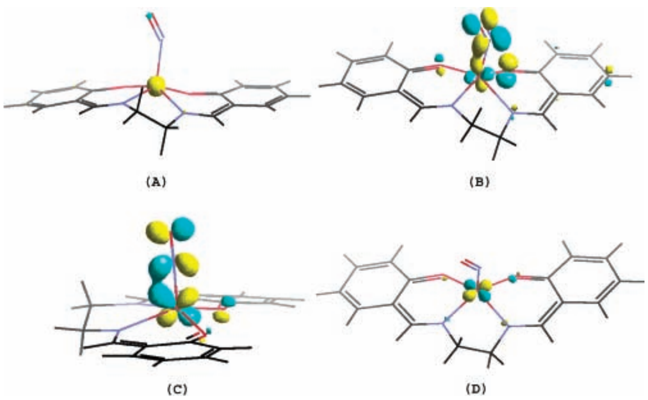

Figure 2. Spin density and MO isosurface representations for the Fe(salen)(NO) HS state. (A) α (yellow) and β (blue) spin densities, (B) β HOMO, (C) β HOMO-1, and (D) α HOMO (contour values = +0.6, ±0.1, ±0.1, and ±0.2 au, respectively).

For Fe(phen)$_2$(NCS)$_2$, the B3LYP-computed Mulliken spin densities $\rho_{\alpha\beta}^{Fe}$ of 3.80e and 0.00e in the RT and LT structures, Table 1, are clear evidence of the presence of $S = 2$ and $S = 0$ states. On the other hand, for Fe(salen)(NO), the DFT results ($\rho_{\alpha\beta}^{Fe} \sim 3.66e$; $\rho_{\alpha\beta}^{Fe} \sim -1.09e$) are clearly indicative of antiferromagnetic coupling between Fe(II) (S = 2) and NO ($S = 1/2$), giving rise to the nominal $S = 3/2$ state in the RT structures, a conclusion which is independent of the disorder of NO in the crystal. Consistent with this picture, the net α spin density in Fe(salen)(NO) is centered on iron while the smaller net β spin density resides on NO, as illustrated in Figure 2A by yellow and blue iso-surfaces, respectively. The derived frontier molecular orbitals (MOs) also support the conclusion of antiferromagnetic coupling, which, in a classical ligand field picture, consists of five iron α electrons, one iron β electron, and one β NO electron. As can be seen in Figure 2B,C, the highest occupied β MO (HOMO) and the β HOMO-1 orbital involve π bonding between the iron d$_{xz}$/d$_{yz}$ and the corresponding NO π^* orbitals and is associated with one iron β electron and one NO β electron. On the other hand, the five frontier α MOs, namely, the α HOMO−α HOMO-4, are primarily composed of the five different 3d orbitals, as exemplified by the α HOMO shown in Figure 2D. These features correspond to the five iron α electrons in a classical ligand field picture. Thus, the classical picture of an Fe(II) ($S = 2$) anti-ferromagnetically coupled with NO ($S = 1/2$) is reproduced in the MO results. In this specific case, due to direct interaction between the four lobes of the d$_{xy}$ orbital and the four atoms in the equatorial ligand plane, d$_{xy}$ becomes the HOMO. As suggested by recent results on the uncommon three-coordinate high-spin ferrous complexes,[34] ligand contributions to the frontier MOs in the HS state of the nitrosyl complex result in a rather small quadrupole splitting (0.35 mm s^{-1}), whereas, in general, high-spin ferrous sites have a ΔE_Q ~3 mm s^{-1}, as found in the HS state of Fe(phen)$_2$(NCS)$_2$ and in ferrous heme.[18] In fact, ΔE_Q decreases linearly with the iron−ligand distance (which corresponds to a monotonic increase in iron−ligand interaction) in the high-spin ferrous model complexes.[35] In sharp contrast, a Mulliken spin density analysis of the nominal $S = 1/2$ state of the LT structure shows that the spin densities here are mainly localized on iron with only a small contribution from the ligands. This can be readily seen in the total spin density iso-surface shown in Figure 3A, which exhibits similarity with other $S = 1/2$ NO−heme model compounds.[18] The shape of the total spin density iso-surface is very similar to that of the lowest β-unoccupied MO (LUMO), shown in Figure 3B, consistent with the results found in other $S = 1/2$ molecular systems.[18,36] When compared with the MO results for the RT structure, these LS results show an increased ligand contribution to the frontier MOs, which is most likely due to shorter iron-ligand contacts in the LT structures (see the geometric parameters given in Table 2). The two original β HOMOs in the HS state (Figure 2B,C) are essentially maintained in the LS state (data not shown); however, the two corresponding α HOMOs change. Specifically, more ligand orbitals contribute to these two α HOMOs (HOMO-2 and HOMO-3) in the LS state, as shown in Figure 3C,D. In this way, the original large ligand spin densities of the β HOMO and the HOMO-1 orbital

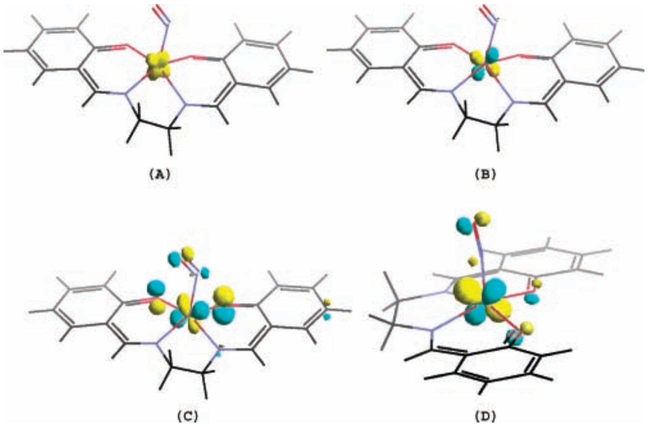

Figure 3. Spin density and MO isosurface representations for the Fe(salen)(NO) LS state. (A) total spin densities, (B) β LUMO, (C) α HOMO-2, and (D) α HOMO-3 (contour values = +0.1, ±0.1, ±0.1, and ±0.1 au, respectively).

in the HS state are in essence paired up with the large ligand spin densities of the two corresponding α HOMOs in the LS state. As a result, there is only a small ligand contribution to the total spin density in the LT structure(s), Figure 3A. The charge density on iron also increases on transition from HS to LS, due to a larger ligand contribution, consistent with the increased $\rho(0)$ values shown in Table 2. This results in a decrease in the ^{57}Fe Mössbauer isomer shifts on transition from a HS to a LS state.

These results show that it is now possible to quite accurately predict ^{57}Fe Mössbauer quadrupole splitting values and isomer shifts in $S = 0$, 1/2, 3/2, and 2 spin-crossover complexes by using density functional theory. This, together with previous successes in predicting Mössbauer quadrupole splitting values and isomer shifts in a broad variety of iron complexes,[18,19] should facilitate the use of combined DFT/Mössbauer investigations in investigating the electronic structures of spin-crossover and other, less conventional, iron complexes.

Acknowledgment. This work was supported by the United States Public Health Service (NIH grant EB00271-24) and by the National Computation Science Alliance (grant MCB-000020N).

References and Notes

(1) Gütlich, P.; Hauser, A.; Spiering, H. *Angew. Chem., Int. Ed. Engl.* **1994**, *33*, 2024−2054.

(2) (a) Cambi, L.; Cagnasso, A. *Atti Accad. Naz. Lincei* **1931**, *13*, 809. (b) Cambi, L.; Szegö, L.; Cagnasso, A. *Atti Accad. Naz. Lincei* **1932**, *15*, 266.

(3) Goodwin, H. A. *Coord. Chem. Rev.* **1976**, *18*, 293−325.

(4) Gütlich, P. *Struct. Bonding (Berlin)* **1981**, *44*, 83−195.

(5) Gütlich, P.; Hauser, A. *Coord. Chem. Rev.* **1990**, *97*, 1−22.

(6) König, E. *Prog. Inorg. Chem.* **1987**, *35*, 527−623.

(7) Ikeue, T.; Ohgo, Y.; Yamaguchi, T.; Takahashi, M.; Takeda, M.; Nakamura, M. *Angew. Chem., Int. Ed.* **2001**, *40*, 2617−2620.

(8) Kahn, O.; Martinez, C. J. *Science* **1998**, *279*, 44−48.

(9) Hayami, S.; Gu, Z.-Z.; Yoshiki, H.; Fujishima, A.; Sato, O. *J. Am. Chem. Soc.* **2001**, *123*, 11644−11650.

(10) (a) Paulsen, H.; Winkler, H.; Trautwein, A. X.; Grünsteudel, H.; Rusanov, V.; Toftlund, H. *Phys. Rev. B* **1999**, *59*, 975−984. (b) Paulsen, H.; Grünsteudel, H.; Meyer-Klaucke, W.; Gerdan, M.; Grünsteudel, H. F.; Chumakov, A. I.; Rüffer, R.; Winkler, H.; Toftlund, H.; Trautwein, A. X. *Eur. Phys. J. B* **2001**, *23*, 463−472.

(11) Paulsen, H.; Duelund, L.; Winkler, H.; Toftlund, H.; Trautwein, A. X. *Inorg. Chem.* **2001**, *40*, 2201−2203.

(12) Chen, G.; Espinosa-Perez, G.; Zentella-Dehesa, A.; Silaghi-Dumitrescu, I.; Lara-Ochoa, F. *Inorg. Chem.* **2000**, *39*, 3440−3448.

(13) Paulsen, H.; Duelund, L.; Zimmermann, A.; Averseng, F.; Gerdan, M.; Winkler, H.; Toftlund, H.; Trautwein, A. X. *Monatsh. Chem.* **2003**, *134*, 295−306.

(14) Chen, G. J.; Liu, R. Z.; Silaghi-Dumitrescu, I.; Espinosa-Perez, G.; Zentella-Dehesa, A.; Lara-Ochoa, F. *Int. J. Quantum Chem.* **2001**, *83*, 60−69.

(15) (a) Grodzicki, M.; Flint, H.; Winkler, H.; Walker, F. A.; Trautwein, A. X. *J. Phys. Chem.* **1997**, *101*, 4202−4207. (b) Nemykin, V. N.; Kobayashi, N.; Chernii, V. Y.; Belsky, V. K. *Eur. J. Inorg. Chem.* **2001**, 733−743. (c) Nemykin, V. N.; Polshina, A. E.; Chernii, V. Y.; Polshin, E. V.; Kobayashi, N. *Dalton* **2000**, 1019−1025.

(16) Godbout, N.; Havlin, R.; Salzmann, R.; Debrunner, P. G.; Oldfield, E. *J. Phys. Chem. A* **1998**, *102*, 2342−2350.

(17) Havlin, R. H.; Godbout, N.; Salzmann, R.; Wojdelski, M.; Arnold, W.; Schulz, C. E.; Oldfield, E. *J. Am. Chem. Soc.* **1998**, *120*, 3144−3151.

(18) Zhang, Y.; Mao, J.; Godbout, N.; Oldfield, E. *J. Am. Chem. Soc.* **2002**, *124*, 13921−13930.

(19) Zhang, Y.; Mao, J.; Oldfield, E. *J. Am. Chem. Soc.* **2002**, *124*, 7829−7839.

(20) Gallois, B.; Real, J.-A.; Hauw, C.; Zarembowitch, J. *Inorg. Chem.* **1990**, *29*, 1152−1158.

(21) König, E.; Madeja, K. *Inorg. Chem.* **1967**, *6*, 48−57.

(22) Haller, K. J.; Johonson, P. L.; Feltham, R. D.; Enemark, J. H.; Ferraro, J. R.; Basile, L. J. *Inorg. Chim. Acta* **1979**, *33*, 119−130.

(23) Wells, F. V.; McCann, S. W.; Wickman, H. H.; Kessel, S. L.; Hendrickson, D. N.; Feltham, R. D. *Inorg. Chem.* **1982**, *21*, 2306−2311.

(24) Debrunner, P. G. In *Iron Porphyrins*; Lever, A. B. P., Gray, H. B., Eds.; VCH Publishers: New York, 1989; Vol. 3, pp 139−234.

(25) Frisch, M. J.; Trucks, G. W.; Schlegel, H. B.; Scuseria, G. E.; Robb, M. A.; Cheeseman, J. R.; Zakrzewski, V. G.; Montgomery, J. A., Jr.; Stratmann, R. E.; Burant, J. C.; Dapprich, S.; Millam, J. M.; Daniels, A. D.; Kudin, K. N.; Strain, M. C.; Farkas, O.; Tomasi, J.; Barone, V.; Cossi, M.; Cammi, R.; Mennucci, B.; Pomelli, C.; Adamo, C.; Clifford, S.; Ochterski, J.; Petersson, G. A.; Ayala, P. Y.; Cui, Q.; Morokuma, K.; Malick, D. K.; Rabuck, A. D.; Raghavachari, K.; Foresman, J. B.; Cioslowski, J.; Ortiz, J. V.; Stefanov, B. B.; Liu, G.; Liashenko, A.; Piskorz, P.; Komaromi, I.; Gomperts, R.; Martin, R. L.; Fox, D. J.; Keith, T.; Al-Laham, M. A.; Peng, C. Y.; Nanayakkara, A.; Gonzalez, C.; Challacombe, M.; Gill, P. M. W.; Johnson, B. G.; Chen, W.; Wong, M. W.; Andres, J. L.; Head-Gordon, M.; Replogle, E. S.; Pople, J. A. *Gaussian 98*, revision A.9; Gaussian, Inc.: Pittsburgh, PA, 1998.

(26) Dufek, P.; Blaha, P.; Schwarz, K. *Phys. Rev. Lett.* **1995**, *75*, 3545−3548.

(27) Mao, J.; Zhang, Y.; Oldfield, E. *J. Am. Chem. Soc.* **2002**, *124*, 13911−13920.

(28) Wachters, A. J. H. *J. Chem. Phys.* **1970**, *52*, 1033−1036. Wachters, A. J. H. IBM Technology Report RJ584. International Business Machines Corp.: Riverton, NJ, 1969.

(29) Becke, A. D. *J. Chem. Phys.* **1993**, *98*, 5648−52.

(30) Lee, C.; Yang, W.; Parr, R. G. *Phys. Rev. B* **1988**, *37*, 785−789.

(31) Becke, A. D. *Phys. Rev. A* **1988**, *38*, 3098−3100.

(32) Perdew, J. P.; Burke, K.; Wang, Y. *Phys. Rev. B* **1996**, *54*, 16533−16539.

(33) (a) Biegler-König, F. *AIM2000*, version 1.0; University of Applied Science: Bielefeld, Germany. (b) Bader, R. F. W. *Atoms in Molecules: A Quantum Theory*; Oxford University Press: Oxford, 1990.

(34) (a) Andres, H.; Bominaar, E. L.; Smith, J. M.; Eckert, N. A.; Holland, P. L.; Münck, E. *J. Am. Chem. Soc.* **2002**, *124*, 3012−3025. (b) MacDonnell, F. M.; Ruhlandt-Senge, K.; Ellison, J. J.; Holm, R. H.; Power, P. P. *Inorg. Chem.* **1995**, *34*, 1815−1822.

(35) Zhang, Y.; Oldfield, E. Unpublished results.

(36) George, S. D.; Metz, M.; Szilagyi, R. K.; Wang, H.; Cramer, S. P.; Lu, Y.; Tolman, W. B.; Hedman, B.; Hodgson, K. O.; Solomon, E. I. *J. Am. Chem. Soc.* **2001**, *123*, 5757−5767.